The Effect of Forebody Geometry on Turbulent Heating and Thermal Protection System Sizing for Future Mars Mission Concepts

James L Brown, Ph.D.
Reacting Flow Environments Branch, MS230-2
NASA Ames Research Center
Moffett Field, CA 94035
jameslbrown@mail.arc.nasa.gov

Abstract

Past Mars entry missions have made extensive use of 70° sphere-cone forebody heatshields. This shape was chosen for its aerodynamic stability during direct entry, either ballistic or low L/D trajectories. Historic missions, including Viking in 1976, Pathfinder in 1997, and Mars Rover in 2004, have provided a large aerodynamic and aerothermodynamic database for the 70° sphere-cone shape that perpetuates continued use for future Mars missions. Using 3D Real-Gas Navier-Stokes simulations, we show that once turbulent heating occupies a significant portion of the mission trajectory, undesireable aerothermodynamic properties arise associated with the 70° sphere-cone heatshield geometry. As an additional consideration, the pitch angle to achieve high L/D of a Mars aerocapture trajectory mitigates the stability justification for the 70° sphere-cone. This suggests that alternative forebody geometries should be considered for future Mars missions.

Introduction

Future Mars mission concepts now include the use of larger diameter entry vehicles capable of aerocapture maneuvers. Associated with large diameter Mars vehicle concepts is the issue of heatshield boundary layer transition to turbulence early in the aerocapture maneuver. High heating levels associated with turbulent flow are expected throughout most of the atmospheric portion of the trajectory. We find that the 70° sphere-cone heatshield geometry[1-3], with a pitch angle set to accomplish aerocapture, to be particularly ill-behaved with respect to heat levels once turbulent transition occurs. On the leeside of the heatshield, the turbulent heating bump factor can reach as high as 6, causing the leeside turbulent heating to exceed even the heating level at the laminar stagnation point. This turbulent heating behaviour for the 70° sphere-cone is seen both in Navier-Stokes solutions for the present work and in experiments carried out in the Cal Tech T5 facility in support of the Mars Science Lab mission, see Wright, et.al.[4].

In this paper, we consider the origins of the observed excess heating associated with turbulent flow over the leeward 70° sphere cone heatshield and, furthermore, examine an alternative ellispoidal heatshield geometry chosen so as to match the 70° sphere-cone diameter and aerodynamic lift and drag. For the latter geometry, transition to turbulence occurs predominantly over the leeside of the heatshield leaving the stagnation point laminar, but with turbulent heating bump factor on the leeside reaching only approximately three. As a consequence, a significant potential reduction in forebody heatshield TPS mass can be achieved relative to that required for a 70° sphere-cone.

Discussion

As an example of this turbulent heating effect, Fig. 1 depicts heatshield surface results obtained using the DPLR Real-Gas Navier-Stokes code[4] for the peak heating time of a trajectory characteristic of a Mars aerocapture mission. Fig. 1 includes pressure contour lines in black and surface streamlines in red. For this trajectory point, the 70° sphere-cone is at a 16° angle of attack and a 0.24 aerodynamic L/D (Lift/Drag). Navier-Stokes solutions were obtained for both laminar and turbulent flow over the heatshield, using an 8-species Mars atmosphere chemistry model. All heating results in this paper are normalized by Qref, the peak laminar heating for this 70° sphere cone at this trajectory point. Fig. 2 shows the boundary layer momentum thickness for the laminar solution. Using as a criterion for turbulence transition as occuring when the laminar boundary layer momentum thickness Reynolds number, Re_θ, exceeds 200, we see that the stagnation point and windward portion of the heatshield remain laminar, while the leeside of the heatshield becomes turbulent. Fig. 1 shows both the laminar (the

figure's left half) and turbulent (the figure's right half) heating levels obtained from the Navier-Stokes solver. As can be seen, turbulent peak heating actually occurs on the leeward-most shoulder far in excess of the stagnation point heating level, with a turbulent heating bump factor, defined as (turbulent Qw)/(laminar Qw), approaching 6 along the leeward centerline.

This turbulent heating effect associated with the 70° sphere-cone geometry suggests that when turbulent transition occurs early in the trajectory, a search for an alternative heatshield geometry may yield a more benign design heating pulse, both integrated and peak levels, with a possibility for relatively lighter density TPS materials and lower forebody TPS mass.

In order to explore this potential, we consider a family of ellipsoid heatshield geometries with parameterization configured so as to match the diameter and aerodynamic lift and drag properties of the 70° sphere-cone heatshield at hypersonic velocities for the Martian atmosphere. The matching of hypersonic aerodynamics was accomplished using a modified Newtonian method for both the 70° sphere-cone and the prototype ellipsoidal shape. Fig. 3 shows the height variation with radius of the resulting axisymmetric ellipsoidal shape as compared to the 70° sphere-cone.

Fig. 4 depicts the ellipsoidal heatshield heating obtained by the DPLR Navier-Stokes solver for the same trajectory conditions as for the 70° sphere-cone heating shown in Fig. 1. Fig. 4 includes pressure contour lines in black and surface streamlines in red. Fig. 5 shows the boundary layer momentum thickness for the ellipsoidal heatshield at this trajectory point.

For the ellipsoidal heatshield, transition occurs on the leeward side of the heatshield similar to the 70° sphere-cone. The laminar heating levels for the 70° sphere-cone and the ellipsoidal heatshield are comparable. However, the peak turbulent heating for the ellipsoid heatshield is at a much reduced level relative to the 70° sphere-cone. The turbulent peak heating for the ellipsoidal heatshield is at a Qw/Qref of 1.63 compared to 3.23 for the 70° sphere-cone, a reduction of nearly 50%.

The high leeside turbulent heating for the 70° sphere-cone appears related to a stronger than expected turbulent viscous-inviscid interaction that occurs for this shape on the heatshield leeside. For a thin boundary layer, inviscid regions are insensitive to growth of the boundary layer. Once boundary layer growth begins to affect the pressure field imposed by the inviscid flow over the viscous region, a viscous-inviscid interaction is said to have occurred. Typical interaction regions include separated regions and shock/boundary layer interactions where wall shear stress and heating can be significantly affected by the interaction. The exact nature of the present interaction is not fully understood, but observations can be made.

To examine the effects of this viscous-inviscid interaction, Fig. 6 and 7 show the boundary layer thickness color contours for the 70° sphere-cone and the ellipsoidal heatshields, respectively. Both laminar and turbulent results are given in these figures. The single black contour line in each figure gives the trace of where the boundary layer edge Mach number, Me, equals 1. Note in Fig. 6, for the leeward portion of the 70° sphere-cone heatshield, that the turbulent Me=1 contour line is changed in position significantly relative to the laminar Me=1 contour line. This corresponds to where the turbulent boundary layer thickness has considerably increased over the laminar thickness. However, Fig. 7 shows this effect on the Me=1 contour line as much less dramatic for the ellipsoidal heatshield.

Fig. 8 through 11 explores the differing strength of this effect for the 70° sphere-cone compared to the ellipsoidal heatshield. These plots give the variation of the boundary layer edge Mach number, wall pressure, boundary layer thickness and convective heating along the centerline, Y=0, of the two heatshields. Obvious is that there is a significant change in the turbulent relative to the laminar solution along the leeward side of the 70° sphere cone heatshield, but this is not true for the ellipsoidal heatshield. There are virtually no differences in the edge Mach number and wall pressure plots for the laminar vs turbulent ellipsoidal heatshield solutions. And yet, the small difference in the wall pressures along the leeward side, turbulent vs laminar, of the 70° sphere-cone is associated with a very substantial change in edge Mach number.

The unusual centerline heating results of Fig. 11, in particular, has experimental support in that similar results for laminar vs. turbulent heating were also obtained for the 70° sphere-cone in the T5 tunnel of CalTech as reported by Wright, et.al.[4] where the turbulent heating bump factor also approached 6 on the leeside centerline of the 70° sphere-cone being tested.

These several observations are manifestations of the unexpected sensitivity of an interaction ocurring between the viscous turbulent boundary layer and the thin inviscid region between the boundary layer and the bow shock in this region for the 70° sphere-cone.

The effects manifest in the viscous-inviscid interaction along the 70° sphere-cone leeside originate for two reasons. The first is that along the leeward centerline the turbulent boundary layer thickness is a significant fraction of the shock standoff distance. The second is the turbulent boundary layer in this region is efficiently entraining, or "swallowing", an energetic entropy layer that occupies much of the inviscid region between the boundary layer and the bow shock. The entropy layer, of course, is an inviscid but rotational region that arises in the presence of a curved bow shock.

Fig. 12 presents, for the leeward centerline (Y=0, Z>0) pitch plane of the 70° sphere-cone, color-shaded contours of the total enthalpy, along with the approximate bow shock position depicted by a solid black line. Both laminar and turbulent solutions are given. The viscous boundary layer region shows clearly in the total enthalpy color contours, since the total enthalpy does not change across the shock nor in the freestream. Fig. 13 supplements Fig. 12 with individual profiles at a typical station, (Y=0, Z/R~3/4), along this same 70° sphere-cone leeside centerline, of the laminar and turbulent normalized velocity, U/U_∞ and normalized total enthalpy, $(H-H_{wall})/(H_\infty-H_{wall})$ as a function of the distance from the wall, Yn/R. Fig. 12 and 13 show the turbulent boundary layer in this region to be considerably thicker than the laminar boundary layer, but is very full with a steep gradient near the surface and with an extensive "wake" region. The turbulent boundary layer edge is best found in Fig. 13 by examination of the normalized total enthalpy at Yn/R~0.018. The turbulent solution bow shock is at Yn/R~0.06. The turbulent boundary layer occupies 30% of the bow shock standoff distance. The bow shock is actually closer to the surface for the turbulent relative to the laminar solution by approximately 7%. Also, the entropy layer edge can best be seen in the velocity profiles of Fig. 13 at Yn/R~0.028, about 47% of the bow shock standoff distance. The turbulent boundary layer is in the process of entraining the rotational entropy layer. The vorticity inherent to an entropy layer is favorable to rapid production of turbulent kinetic energy. As the turbulent structures span the boundary layer, this energizes the inner portion of the boundary layer, leading to a full velocity profile, a higher wall shear stress and higher heat transfer.

The observed increase in turbulent boundary layer edge Mach number for the 70° sphere-cone leeside occurs, not as a result of acceleration, but because the turbulent boundary layer edge moves outwards into the higher Mach number entropy layer as part of the entrainment process. This entrainment process is rapid, being nearly complete by the time the leeward shoulder is reached.

Fig. 14 shows contours of the normalized wall shear stress and reinforces the observation that the wall shear stress and heat transfer undergo a significant increase in this leeside centerline region of the 70° sphere-cone as a result of the entropy swallowing process.

These unusual effects are not observed to occur with the ellipsoidal heatshield. Although there is an increase in thickness for the turbulent boundary layer relative to the laminar boundary layer (Fig. 10), no discernible difference in the wall pressures (Fig. 9) are seen for the turbulent vs. laminar ellipsoid heatshield, and the edge Mach numbers (see Fig. 8) are unaffected as well. Further, the turbulent heating bump factor over most of the ellipsoidal heatshield remains at a level of approximately 3, more characteristic of an "acreage" or weak interaction turbulent heating bump factor. Unlike the 70° sphere cone, the bow shock for the ellipsoidal heatshield stands considerably further off the surface, so that the increase in turbulent boundary layer thickness does not lead to the types of viscous-inviscid interaction effects seen with the 70° sphere-cone.

To compare thermal protection system, TPS, sizing for the baseline 70° sphere-cone and the alternative ellipsoid heatshield, the heat pulse for a typical 70° sphere-cone Mars aerocapture trajectory shown in Fig. 15 is used in conjunction with the FIAT material response code, see Chen and Milos[5]. Loomis suggests in [6] a convenient curve fit procedure where the form $q=a\rho^m V^n$ is assumed and the coefficients a,m and n are found from fitting a limited number of heat transfer solutions along a specified trajectory. Loomis fits for the heating pulse for both the 70° sphere-cone and the ellipsoidal heatshields are shown based on the same vehicle atmospheric entry trajectory. The same trajectory (velocity and altitude vs time) would appy to both heatshields since the ellipsoidal heatshield was configured to match the aerodynamic lift and drag of the 70° sphere-cone heatshield.

Due to the high heating level for this trajectory of the 70° sphere-cone, PICA (Phenolic Impregnated Carbon Ablator, see Tran, et.al.[7]) is chosen as a suitable baseline TPS material. A simplified constant thickness TPS approach is used for the baseline heatshield giving an unmargined mass of 232 Kg for the PICA baseline 70° sphere-cone heatshield. For the 70° sphere-cone, proper center-of-gravity placement is aggravated by the leeside peak turbulent heating were variable thickness heatshield to be used.

TPS sizing was also carried out for the ellipsoid heatshield. The approximately 50% lower peak heat transfer enabled consideration of lighter TPS materials such as SLA-561v (see Covington, et.al.[8]) for the ellipsoid heatshield. Further, the lower heating pulse appropriate to the ellipsoidal heatshield shown in Fig. 15 is used for the ellipsoidal heatshield TPS sizing. TPS sizing for the SLA-561v ellisoid heatshield gives an unmargined forebody heatshield TPS mass of 64 Kg. Fig. 16 compares this estimate for unmargined mass of the SLA-561v ellipsoidal heatshield with the 232 Kg for the unmargined mass for the PICA baseline 70° sphere-cone heatshield.

The considerable saving in TPS mass for the ellipsoidal heatshield relative to the 70° sphere-cone is the consequence not only of the reduction in thickness of the heatshield but also that a switch to the lighter density SLA 561v was enabled due to the much lower peak heating level. The reduction in peak heating by approximately 50% for the ellipsoidal heatshield relative to the 70° sphere-cone thus leads to forebody heatshield with only 27% of the TPS mass.

This particular example emphasizes both the non-linearity of TPS mass sizing with applied heat load and the importance of heatshield shape in reducing the entry integrated heat load.

Concluding Remarks

A more thorough aerodynamic stability and aerothermodynamic analysis of the ellipsoid heatshield, followed by experimental validation, would be required before its use could be confidently recommended for a Mars mission. We stress that no optimization of the ellipsoidal heatshield geometry was attempted, only that the hypersonic lift and drag levels were matched to the baseline 70° sphere-cone heatshield.

Clearly demonstrated in this paper is that with an increase in probe size anticipated for future Mars missions, once the flow over the 70° sphere-cone heat shield becomes turbulent, a significant penalty in excessive heating is associated with the 70° sphere-cone geometry. This appears to be associated with a weak viscous-inviscid interaction arising from the "swallowing" of the entropy layer over the leeside heat shield by the turbulent boundary layer leading to energizing the inner portion of the turbulent boundary layer, with consequent high wall shear stress and heat transfer. This problem is seen not to occur with at least one alternative heatshield shape, that of a modified ellipsoid. As a result, demonstrated in this brief analysis, there is sufficient potential to justify further exploration of heatshield geometries that are alternatives to the classic 70° sphere-cone for use in future Mars missions.

Acknowledgements

This work was supported by Michelle Munk of the NASA In-Space Propulsion program. The TPS sizing reported in this paper for the 70° sphere-cone and ellipsoidal heatshield were accomplished by Y.-K. Chen and S. Sepka of Ames Research Center.

References

1. Viking Lander System, Primary Mission Performance Report, NASA CR-145148, Martin-Marietta, April 1977.
2. Milos, F.S. and Chen, Y.-K., Mars Pathfinder Entry Temperature Data, Aerothermal Heating, and Heatshield Material Response, *Journal of Spacecraft and Rockets*, Vol. 36, No. 3, May-June 1999.
3. Roncoli, R.B., and Ludwinski, J.M., Mission Design Overview for the Mars Exploration Rover Mission, AIAA 2002-4823.
4. Wright, M.J., Olejniczak, J., Brown, J.L., Hornung, H.G. and Edquist, K.T., Computational Modeling of T5 Laminar and Turbulent Heating Data on Blunt Cones, Part 2: Mars Applications, AIAA 2005-0177, Jan. 2005.
5. Chen, Y.-K., and Milos, F.S., Ablation and Thermal Response Code for Spacecraft Heatshield Analysis, *Journal of Spacecraft and Rockets*, Vol. 36, No. 3, May-June 1993.
6. Olynick, D., Loomis, M., Chen, Y.-K.,

Venkatapathy, E. and Allen, G., New TPS Design Strategies for Planetary Entry Vehicle Design, AIAA 99-0348, Jan. 1999.

7. Tran, H.K., Johnson, C.E., Rasky, D.J., Hui, F.C.L., Tsu, M.-T. and Chen, Y.-K., Phenolic Impregnated Carbon Ablators (PICA) for Discovery Class Missions, AIAA 96-1911, June 1996.

8. Covington, M.A., Heinemann, J.M., Goldstein, H.E., Chen, Y.-K., Sailinas, T.-S., Balboni, J.A., Olejniczak, J., and Martinez, E.R., Performance of a Low Density Ablative Heat Shield Material, AIAA 2004-2273, June 2004.

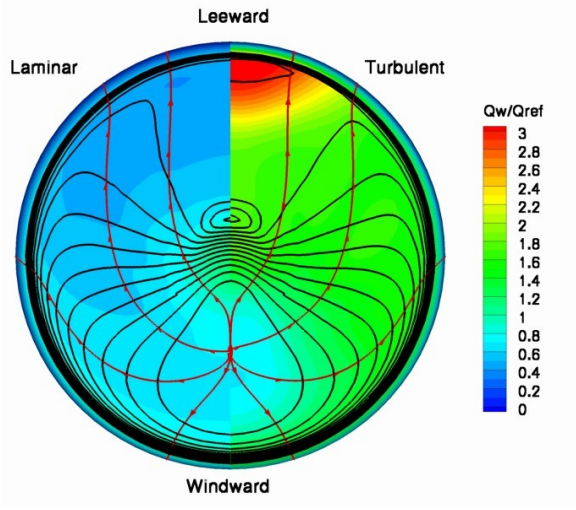

Fig. 1. Convective Heat Transfer for 70° Sphere-Cone Heatshield. 16° angle of attack, L/D=0.24, Peak Heating Trajectory Point. Surface streamlines in red. Pressure contour lines in black.

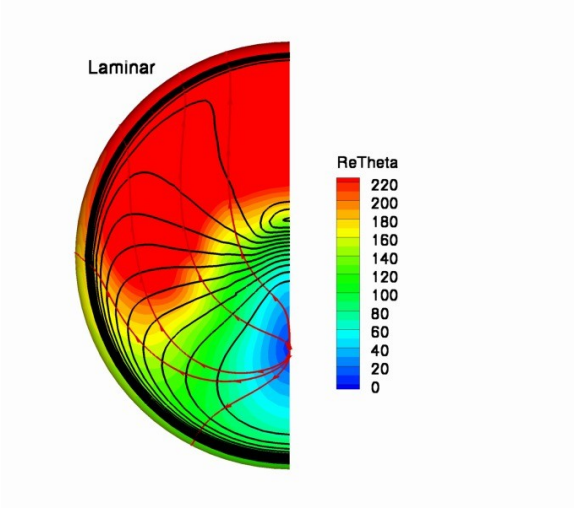

Fig. 2. Laminar Boundary Layer Momentum Thickness for 70° Sphere-Cone Heatshield.

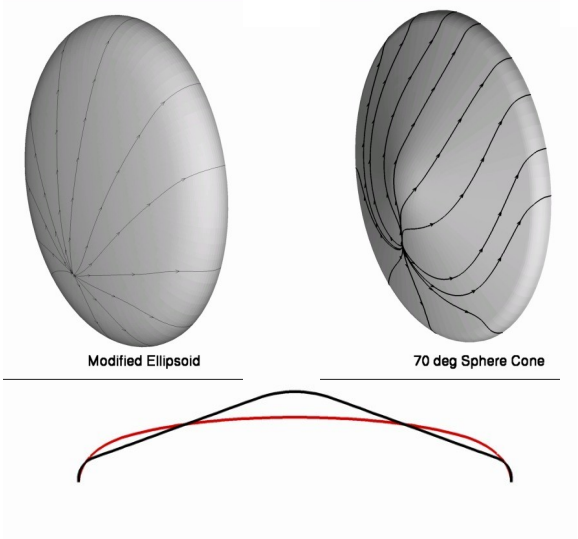

Fig. 3. Ellipsoidal (red) Heatshield Shape Comparison with 70° Sphere-Cone (black).

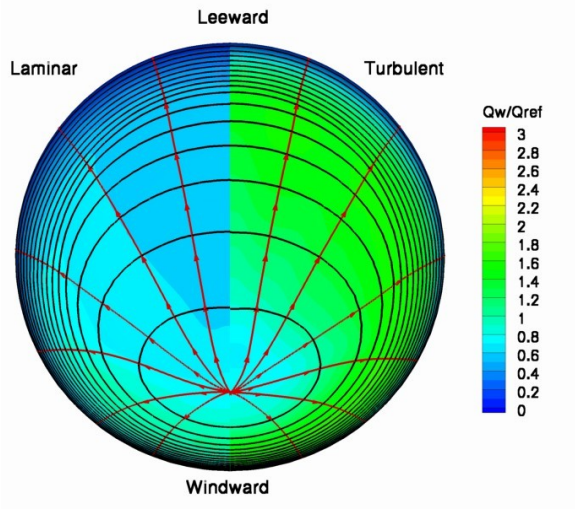

Fig. 4. Convective Heat Transfer for Ellipsoidal Heatshield, 16° angle of attack, L/D=0.24, Peak Heating Trajectory Point.

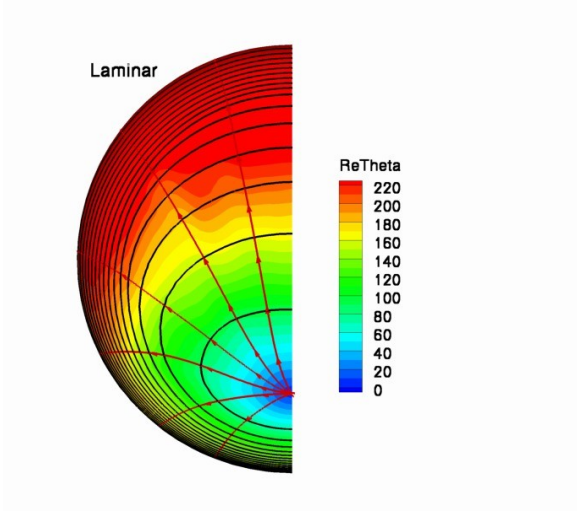

Fig. 5. Laminar Boundary Layer Momentum Thickness for Ellipsoidal Heatshield.

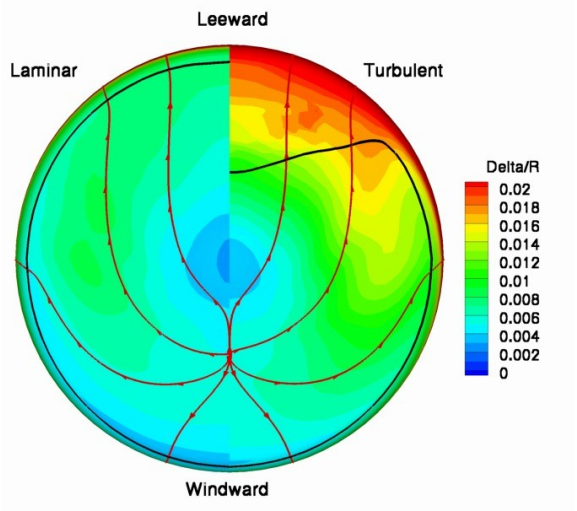

Fig. 6. Boundary Layer Thickness for 70° Sphere-Cone Heatshield. Mach 1 contour line in black, Surface Streamlines in red.

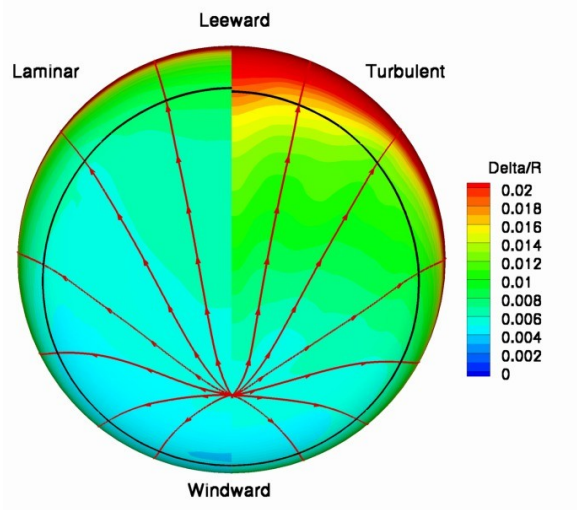

Fig. 7. Boundary Layer Thickness for Ellipsoidal Heatshield. Mach 1 contour line in black. Surface Streamlines in red.

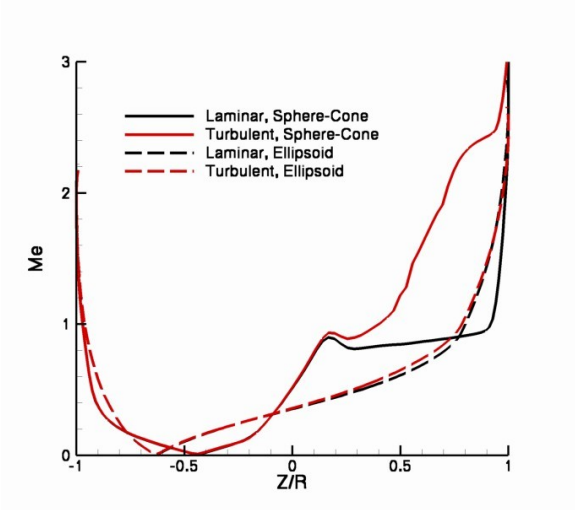

Fig. 8. Boundary Layer Edge Mach number variation along the Y=0 centerline for the 70° Sphere-Cone and Ellipsoidal Heatshields.

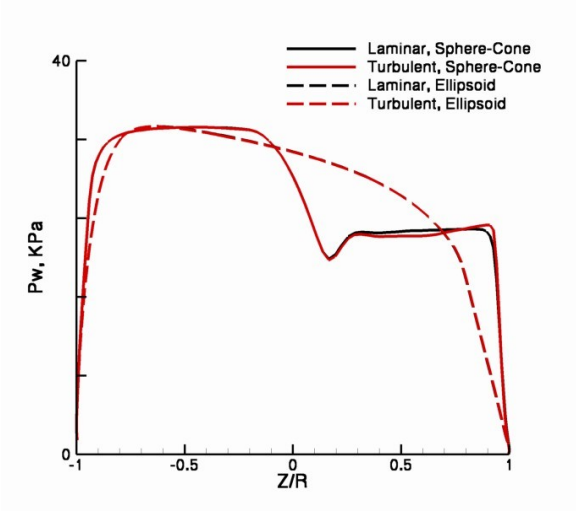

Fig. 9. Wall Pressure variation along the Y=0 centerline for the 70° Sphere-Cone and Ellipsoidal Heatshields.

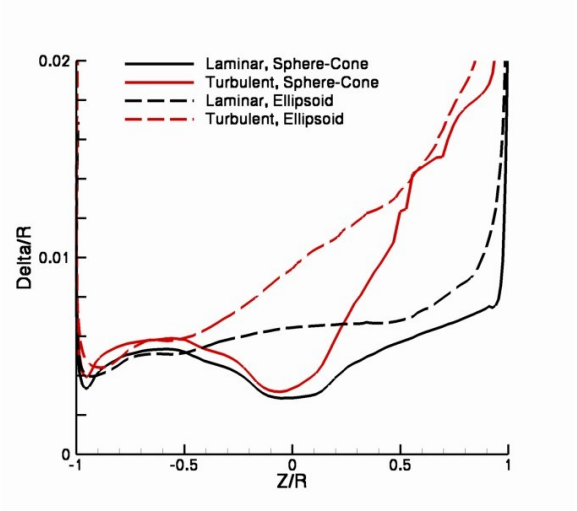

Fig. 10. Boundary Layer Thickness variation along the Y=0 centerline for the 70° Sphere-Cone and Ellipsoidal Heatshields.

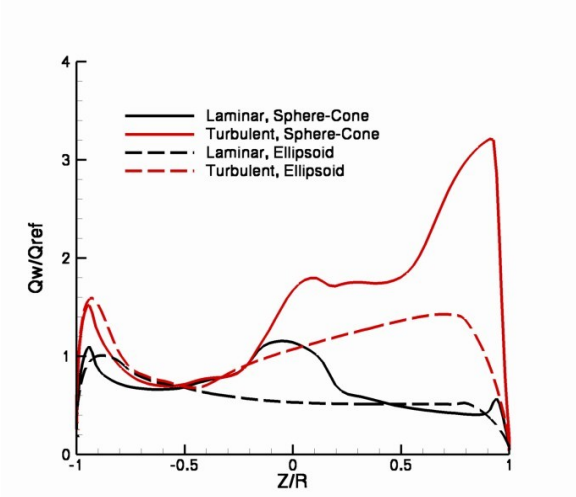

Fig. 11. Convective Heat Transfer variation along the Y=0 centerline for the 70° Sphere-Cone and Ellipsoidal Heatshields.

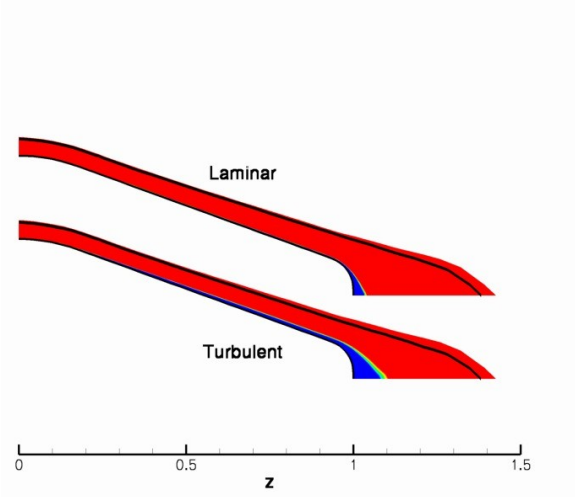

Fig. 12. Total Enthalpy Color Contours for Laminar and Turbulent Leeward Pitch Plane of 70° Sphere-Cone Heatshield. Bow shock location is depicted by black line.

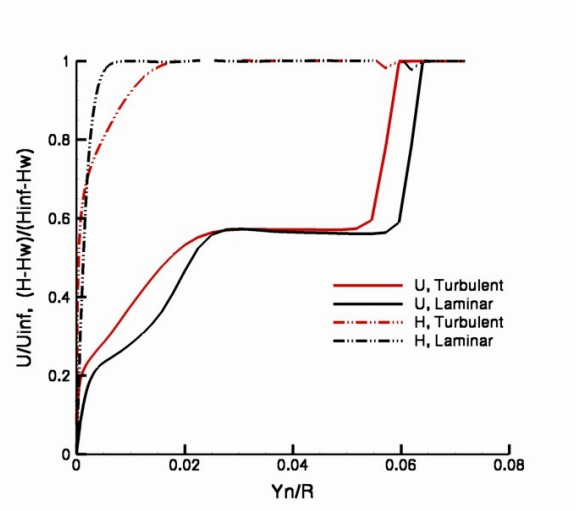

Fig. 13. Normalized Velocity and Total Enthalpy profiles for 70° Sphere-Cone leeward centerline (Y=0, Z/R=3/4)

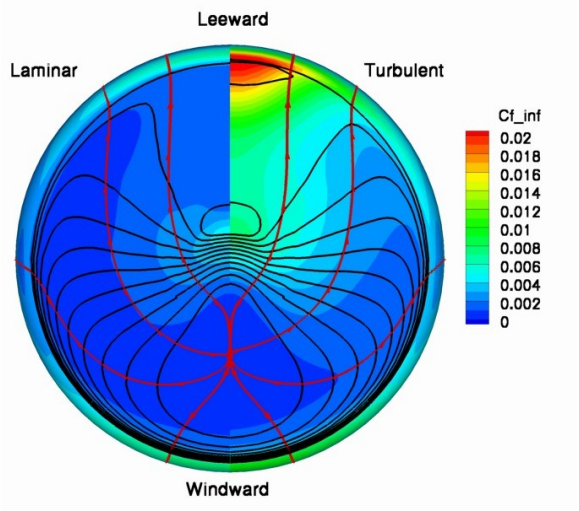

Fig. 14. Surface Shear Stress distribution for 70° Sphere-Cone. Normalized by 0.5(ρU^2)∞.

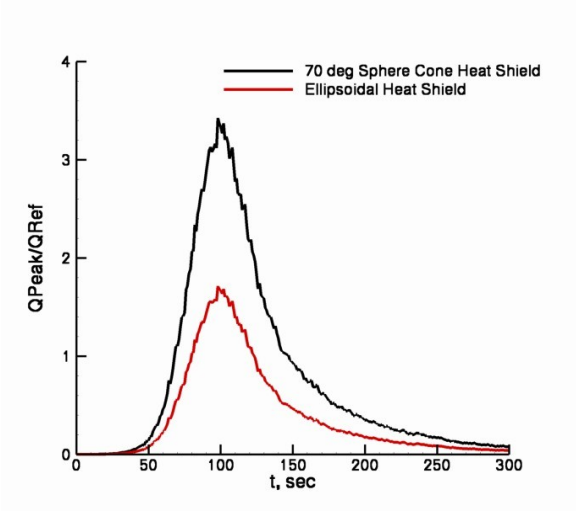

Fig. 15. Peak Heating Pulse for Ellipsoidal and 70° Sphere-Cone Heatshields, including turbulence, Mars Aerocapture Trajectory.

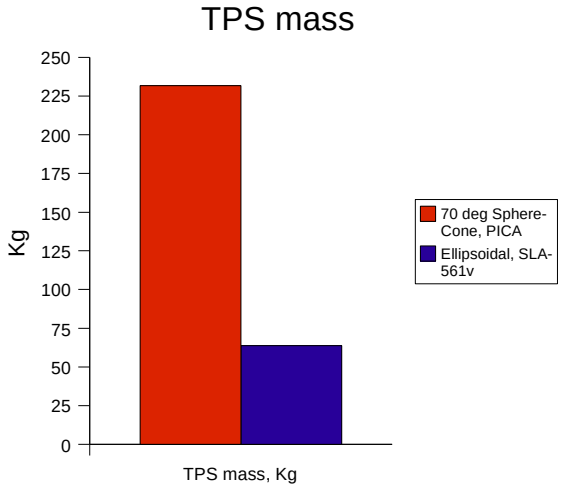

Fig. 16. TPS Sizing for Ellipsoidal vs 70° Sphere-Cone Heatshield.